https://doi.org/10.5194/egusphere-2025-5999
Preprint. Discussion started: 7 January 2026

Concurrent hydrological closure and hominin presence in the Early Pleistocene Nihewan Basin (northern China): insights from stable isotopes

Ahmed H. Moghazi[a, e]*, Hailong Zhao[b]*, Chengjun Zhang[c], Birgit Schröder[d], Steffen Mischke[a]

[a] Institute of Earth Sciences, University of Iceland, Reykjavík, Iceland
[b] School of Archaeology and Museology, Liaoning University, Shenyang, Liaoning, China
[c] College of Earth Sciences & Key Laboratory of Mineral Resources in Western China, Lanzhou University, Lanzhou, Gansu, China
[d] Helmholtz Centre Potsdam, German Research Centre for Geosciences, Potsdam 14473, Germany
[e] Geology Department, Faculty of Science, Aswan University, Aswan, 81528, Egypt

Corresponding Authors: *Ahmed H. Moghazi (aha37@hi.is), Hailong Zhao (t5009@163.com)

ABSTRACT

The Nihewan Basin in northern China contains rich Early Pleistocene Palaeolithic sites, representing one of the earliest locations of hominins outside Africa. Here, we present the first long-term stable oxygen ($\delta^{18}O_{eq.cal}$) and carbon ($\delta^{13}C_{eq.cal}$) isotope record derived from ostracod shells, preserved in the composite 86.2-m NH-T sediment section at the northeastern part of the basin, with a timeframe between ca. 1.67 and 0.78 Ma. The study aimed at reconstructing the long-term climatic changes and hydrological dynamics of the Early Pleistocene Nihewan Basin and to assess their impact on hominin activities. Unexpectedly, we found a strong covariance of $\delta^{18}O_{eq.cal}$ and $\delta^{13}C_{eq.cal}$ values, clearly suggesting that the basin was mostly hydrologically closed. The dominance of evaporation implies that $\delta^{18}O_{eq.cal}$ shifts track the hydrological state at the section location between closed settings with higher water levels (more standing waters) and open settings with low water levels (more flowing waters) instead of regional changes in precipitation/evaporation ratios alone. Moreover, we observed the concurrence of high $\delta^{18}O_{eq.cal}$ and $\delta^{13}C_{eq.cal}$ values and the increase in the marine-land temperature gradient (ΔT), indicating enhanced East Asian Summer Monsoon (EASM)-driven precipitation which led to wetter climate and increased biogenic productivity. Conversely, low $\delta^{18}O_{eq.cal}$ and $\delta^{13}C_{eq.cal}$ values reflect

https://doi.org/10.5194/egusphere-2025-5999
Preprint. Discussion started: 7 January 2026

decreased EASM-driven precipitation and drier climate and reduced biogenic productivity. The new stable isotope data, combined with the synthetic archaeological record, suggest that hominin activities in the Nihewan Basin mostly coincided with periods of higher $\delta^{18}O_{eq.cal}$ and $\delta^{13}C_{eq.cal}$ values when more standing waters bodies and wetter climate prevailed in the region.

Keywords: Quaternary; Asia; Palaeoclimate; Early humans; Palaeolithic

1. INTRODUCTION

Studying the Early Pleistocene is critical for our understanding of the past global climate variability and its inextricable link to hominin evolution, adaptation, and dispersal (Potts et al. 2020; Yang et al., 2021). From a geoarchaeological perspective, the Nihewan Basin in E Asia represents an especially promising research area due to its well-constrained, continuous sedimentary sequence that preserves an abundance of stone artefacts. Since the 1920s, the basin has been recognized for its long paleontological succession of the Early Pleistocene megafauna, known as the Nihewan Fauna (Teilhard de Chardin and Piveteau, 1930; Qiu, 2000). Later, it becomes a hub of archaeological discoveries at numerous paleoanthropological sites, representing the densest concentration of Early Pleistocene Palaeolithic sites outside Africa (Zhu et al., 2004; Deng et al., 2008; Ao et al., 2013; Tu et al., 2022). The basin contains evidence of the oldest hominin presence in northern China, dating back to ca 1.66 Ma, found at the Majuangou site in the eastern part of the Nihewan Basin (Zhu et al., 2004). This timeframe is approximately the same age as that of the oldest fossil *Homo erectus* cranium of ca. 1.63 Ma, discovered at Gongwangling, north of the Qinling Mountains (Zhu et al., 2015). Based on their palaeoclimate reconstructions, Moghazi et al. (2024b) suggested that the climate patterns of the Nihewan Basin, driven by variations in both the East Asian summer (EASM) and winter monsoon (EAWM) closely align with those observed in the Chinese Loess Plateau (CLP) records in response to global glacial/interglacial cyclicity throughout the Early Pleistocene. This situates the Nihewan sedimentary sequence in a regional context as a climatically sensitive terrestrial archive, comparable to the loess-palaeosol sequences of the CLP and deep-sea sediments for reconstructing Quaternary climate change. These observations collectively highlight the palaeoanthropological and palaeoclimatic significance of the high-resolution sediment record from the Nihewan Basin in E Asia.

https://doi.org/10.5194/egusphere-2025-5999
Preprint. Discussion started: 7 January 2026

Based on the few published $\delta^{18}O_{enamel}$ and $\delta^{13}C_{enamel}$ records of Pleistocene mammalian tooth enamel (Xu et al., 2021, 2023), the environment in the Nihewan Basin underwent a marked transition from wet, closed landscapes dominated by C_3 vegetation before 1.2 Ma to drier, open landscapes with mixed C_3/C_4 vegetation between 1.2 and 1.1 Ma. Moreover, the pollen record shows that the climate of the basin shifted from cold-wet forest to cold-dry grassland during 1.337-1.324 Ma. This was followed by warm, wet conditions with sparse forest cover from 1.324 -1.317 Ma, then warm and humid climate during 1.317-1.312 Ma with forest-dominated environment, and eventually a return to cold, dry grassland from 1.312-1.290 Ma (Yang et al., 2022). Whilst previous efforts have been made, longer-term continuous stable isotope records directly retrieved from strata in the Nihewan Basin and covering the long span of ca. 1.3 Ma of hominin activities in the basin between ca.1.66-0.4 Ma (Zhu et al., 2004; Deng et al., 2008; Dennell, 2013; Pei et al., 2019) are still lacking.

The $\delta^{18}O_{ost}$ and $\delta^{13}C_{ost}$ of carbonate valves of ostracods (small aquatic crustaceans) have been successfully used to reconstruct palaeoclimatic conditions in continental settings (Holmes and Chivas, 2002). Their $\delta^{18}O$ values are used to characterize the hydrology of the host waterbody, regional temperature and evaporation and precipitation changes, water sources, and meltwater or groundwater inflow (Schwalb, 2003). In contrast, atmospheric pCO_2 concentration, primary productivity, modes of organic matter decay, and photosynthetic activity of aquatic plants are recorded in their $\delta^{13}C$ values (Schwalb et al., 2013). Thus, the $\delta^{18}O_{ost}$ and $\delta^{13}C_{ost}$ records from sedimentary sequences in the Nihewan Basin can be a useful tracer for hydrological, temperature and vegetation changes during the Early Pleistocene.

In this study, we present the first long-term $\delta^{13}C_{ost}$ and $\delta^{18}O_{ost}$ records from the 86.2-m composite NH-T section at the northeastern part of the basin, spanning ca. 1.67 to 0.78 Ma. This isotope record is integrated with our previously published grain-size endmember (EM) dataset (Moghazi et al., 2024b) to reconstruct the hydrological conditions in the Nihewan Basin during the Early Pleistocene. Together with the artefactual record syntheses, we attempt to explore the link between the basin's local hydrology and the Early Pleistocene hominin activities.

2. Geological setting and modern climate

The Nihewan Basin is a Late Cenozoic fault-controlled basin situated at the northeastern margin of the CLP, within the Inner Mongolia Plateau and the N China Plain, ca. 150 km NW of

https://doi.org/10.5194/egusphere-2025-5999
Preprint. Discussion started: 7 January 2026

Beijing at 40° N and 114° E (Fig. 1). The basin's formation is linked to the extensional tectonics of the Fen-Wei Graben, due to the northward movement of the Indian subcontinent colliding with the Eurasian plate during the Cenozoic era (Sun, 2005). The basin is characterized by a large valley, ca. 80 km long and 15-20 km wide, with an average elevation of ca. 1000 m. It is surrounded by the Xiong'er Mountain to the N, the Liuleng Mountains to the S, the Fenghuang Mountains to the E and the Guancen Mountain to the SW. The basin encompasses the ENE-striking Datong, Yangyuan, and Yuxian sub-basins.

The "Nihewan Beds" (Barbour, 1924) are up to 700-m thick lacustrine, fluvial, and windblown deposits (Zhou et al., 1991). This sedimentary succession dates back from the Early Pliocene ca. 4.2 Ma to the middle Pleistocene ca. 300 ka based on the palaeomagnetic (Deng et al., 2008; Bi et al., 2022) and luminescence (Han et al., 2016) dating. The Nihewan Formation (Min and Chi, 2003) in the lower part of the "Nihewan Beds" represents the type section of the Early Pleistocene in northern China (Young, 1950). The exposed sediment sections are primarily distributed along the SW-NE trending Sanggan River (Sangkan Ho) and SE-NW trending Huliu River on the Cenjiawan Platform (Barbour et al., 1927) near the northeastern margin of the Nihewan Basin. The Sanggan River, the largest river in the basin, flows from west to east through the Datong and Yangyuan sub-basins whilst its major tributary, the Huliu River, runs through the Yuxian sub-basin.

The Nihewan Basin experiences EAM climate and lies between the temperate semi-humid and semi-arid zones. Winters are cold and long, controlled by the cold Mongolian High, whilst summers are warmer and more humid due to the Pacific High. Based on dataset from the Shijiazhuang meteorological station (1985-2003), ca. 235 km S of the Nihewan Basin, the mean January, July and annual air temperatures are ca. -2, 28 and 14 °C, respectively. Additionally, the mean annual precipitation (MAP) is 542 mm, with the majority falling during the summer months (Global Network for Isotopes in Precipitation (GNIP) database: https://nucleus.iaea.org/wiser). Located on the edge of the EASM influence, the basin represents a mixed zone of C_3 and C_4 plants. Its vegetation varies from warm-temperate deciduous broadleaved forests to semi-arid and arid grasslands (Mu et al., 2015).

3. MATERIALS AND METHODS

3.1. Stable isotope analysis

https://doi.org/10.5194/egusphere-2025-5999
Preprint. Discussion started: 7 January 2026

Material for this study derived from the 86.2-m thick composite NH-T section which resulted from the correlation of three newly exposed individual sediment sections (T1-T3) on the Dachangliang ridge (Fig. 1; Moghazi et al., 2024a). The NH-T section has been assigned an astronomically-tuned age range slightly revised in this study to ca. 1.67-0.78 Ma (Moghazi et al., 2024b). Stable O and C isotopes of ostracod calcite were analyzed for adult valves from a total of 90 samples selected throughout the NH-T section. Due to the absence of a single well-preserved and sufficiently abundant ostracod taxon over the whole sedimentary sequence, isotope measurements were continuously conducted on valves of mixed species assemblages (typically 10-15 valves per sample). These taxa include *Limnocythere flexa*, *Leucocythere* sp. (n= 43 samples) and *Ilyocypris* sp. (n= 41 samples). In the prominent white marl beds where other taxa were absent, valves of *Cytherissa lacustris* (n=6 samples) were exclusively used (Moghazi et al., 2024a). Valves with adhering sand grains and organic matter clumps were cleaned in 1% H_2O_2 with the aid of a fine brush under a stereomicroscope. Following the removal of H_2O_2 with a pipette, the valves were rinsed with ethanol and dried. Stable isotopes of the prepared samples were then measured at the Deutsches GeoForschungszentrum Potsdam (GFZ) using a MAT 253 ThermoFisher Scientific isotope ratio mass spectrometer coupled with an automated Carbonate Kiel IV device. During this process, the carbonate was reacted with 103% phosphoric acid (H_3PO_4) at 70°C to release CO_2. The ratios of $^{18}O/^{16}O$ and $^{13}C/^{12}C$ of the valves were expressed in permille (‰) relative to the VPDB standard, with a $\delta^{18}O$ value of -2.20‰ and a $\delta^{13}C$ value of 1.95‰ assigned to the NBS19 standard, ensuring comparability with published datasets. The analytical precision for the $\delta^{18}O$ and $\delta^{13}C$ values is <0.07‰.

3.1.1. Correction of stable isotopes for vital offsets

It was shown that the biogenic calcite of benthic ostracod valves does not precipitate in isotopic equilibrium with the host water (von Grafenstein et al., 2000). Stable isotope values for different species may have distinct systematic offsets from the values of abiotic, fine-grained bulk carbonate that precipitated under the same conditions due to so-called vital effects (i.e., biological/metabolic processes; Holmes and Chivas, 2002). To calculate the isotopic composition of abiotic calcite $\delta^{18}O_{eq.cal}$ and $\delta^{13}C_{eq.cal}$ which precipitated from host water in isotopic equilibrium, the measured $\delta^{18}O_{ost}$ and $\delta^{13}C_{ost}$ values can be reliably corrected by known species-specific vital offsets (von Grafenstein et al., 1999). Accordingly, the stable isotope data for *Limnocythere flexa*

https://doi.org/10.5194/egusphere-2025-5999
Preprint. Discussion started: 7 January 2026

and *Leucocythere* sp. were corrected based on published offsets for *Limnocythere inopinata* because vital offsets seem to be constant for individual genera or even families. The previously reported vital offsets for *L. inopinata* are 0.78‰ for $\delta^{18}O_{ost}$ and -1.18‰ for $\delta^{13}C_{ost}$ values (von Grafenstein et al., 1999). *Cytherissa lacustris* shows species-specific offsets of 1.49‰ for $\delta^{18}O_{ost}$ and -0.13‰ for $\delta^{13}C_{ost}$ values, and vital offsets of 0.32‰ for $\delta^{18}O_{ost}$ and 3.03‰ for $\delta^{13}C_{ost}$ values were determined for *Ilyocypris* sp., as calculated from the average difference between the measured $\delta^{13}C_{ost}$ and $\delta^{18}O_{ost}$ values of *Eucypris mareotica* and *Ilyocypris sebeiensis* (Mischke et al., 2008). For most parts of the NH-T section, the vital offset of the dominant species was used. However, in stratigraphic intervals of the NH-T section where multiple species are dominantly present in roughly equal proportions, composite offsets were calculated. The calculation of these composite offsets was based on the average weighing related to the number of valves for each species. The combination of *C. lacustris* with *Ilyocypris* sp. resulted in an average correction of 0.59‰ for $\delta^{18}O_{ost}$ and -1.58‰ for $\delta^{13}C_{ost}$, whilst *L. flexa* combined with *Ilyocypris* sp. led to adjustments of 0.23‰ for $\delta^{18}O_{ost}$ and -2.11‰ for $\delta^{13}C_{ost}$ values.

4. RESULTS

4.1. $\delta^{18}O_{ost}$ and $\delta^{13}C_{ost}$ data

The raw $\delta^{18}O_{ost}$ values of the analyzed four ostracod species in the NH-T sediment section range from -11.0 to -0.6 ‰ (VPDB) with an average of -3.9 ‰ (n = 93). The raw $\delta^{13}C_{ost}$ values vary between -8.5 and 1.3 ‰ (VPDB) with an average of -2.3 ‰ (n = 93) (Fig. 2). The $\delta^{18}O_{ost}$ and $\delta^{13}C_{ost}$ data show a covariance with a regression coefficient (*r*) value of 0.7 (Fig. 3).

In the lower part of NH-T section at 0.0-15.5 m, the wetland-lake interval defined by Moghazi et al. (2024a) shows average $\delta^{18}O_{eq.cal}$ and $\delta^{13}C_{eq.cal}$ values of -3.8 and -2.6 ‰, respectively (Fig. 2). In the overlying wetland interval at 15.5-30.4 m, the average $\delta^{18}O_{eq.cal}$ and $\delta^{13}C_{eq.cal}$ values are -5.6 and -4.7 ‰, respectively. Higher up, the wetland-alluvial plain interval at 30.4-39.3 m, shows average $\delta^{18}O_{eq.cal}$ and $\delta^{13}C_{eq.cal}$ values of -4.2 and -3.1 ‰, respectively. The subsequent wetland-lake interval at 39.3-55.8 m, is characterized by average $\delta^{18}O_{eq.cal}$ and $\delta^{13}C_{eq.cal}$ values of -3.9 and -1.2 ‰. In the wetland-alluvial plain interval at 55.8-74.0 m, the average $\delta^{18}O_{eq.cal}$ and $\delta^{13}C_{eq.cal}$ values are -4.8 and -4.1 ‰, respectively. Eventually, the uppermost wetland-lake interval at 74.0-86.2 m, contains samples with average $\delta^{18}O_{eq.cal}$ and $\delta^{13}C_{eq.cal}$ values of -3.3 and -2.9 ‰, respectively.

https://doi.org/10.5194/egusphere-2025-5999
Preprint. Discussion started: 7 January 2026

5. DISCUSSION

5.1. Interpretation of the $\delta^{18}O_{ost}$ and $\delta^{13}C_{ost}$ records

The high covariance between $\delta^{18}O_{ost}$ and $\delta^{13}C_{ost}$ signals with *r* value of 0.7 in the NH-T sediment section clearly suggests that the Early Pleistocene Nihewan Basin had hydrological characteristics similar to those typically observed in closed basin settings (Talbot, 1990). The overall range of $\delta^{18}O_{eq.cal}$ values is from -11.3 to -1.5 ‰ (average -4.3 ‰), whilst $\delta^{13}C_{eq.cal}$ values range from -11.5 to 2.5 ‰ (average -3 ‰). If the equation of Kim and O'Neil (1997) with the determined range of $\delta^{18}O_{eq.cal}$ values from the NH-T section for the formed carbonate and an assumed $\delta^{18}O$ value of -8 ‰ (SMOW) for the host water ($\delta^{18}O$ value of modern precipitation at the Shijiazhuang meteorological station) is solved for the water temperature, unrealistically low values mostly below 0 °C with an average of -1.7 °C are inferred. Ostracod valves must have formed at higher water temperatures. In modern lakes on the southern Tibetan Plateau, living ostracods were abundant in waters of 12-13.8 °C but not in colder waters (Börner et al., 2017). In addition, significantly higher air temperatures were inferred from Early Pleistocene pollen records of the Nihewan Basin. Zhang et al. (2020) reconstructed average air temperatures of < 6 °C during cold periods and > 8 °C during warm periods. Therefore, temperature was apparently not the main controlling parameter which resulted in the determined $\delta^{18}O_{eq.cal}$ values for the NH-T section. Thus, the relatively large range of the $\delta^{18}O_{eq.cal}$ values (9.8 ‰ for the total range), the overall correlation of the $\delta^{18}O_{ost}$ and $\delta^{13}C_{ost}$ values, and also the low ostracod diversity of the NH-T section in comparison to modern freshwater lakes in the region (Zhai et al., 2011) suggest that water in the Early Pleistocene Nihewan Basin was mainly controlled by the precipitation/evaporation ratio or changing effective moisture similar to typical closed-basin lakes. This inference is supported by sedimentological and geochemical analyses of Li et al. (2000) who suggested that the Nihewan paleolake was "weak-saline" to "semi-saline". Additionally, the stratigraphic intervals of the NH-T section with the higher $\delta^{18}O_{ost}$ values at ca. 7 and 27 m are characterized by the dominant occurrence of *Heterocypris salina*. *Heterocypris salina* typically lives in small and marginally saline inland and coastal waters and was documented to form large populations in saline sulfurous springs (Fig. 2; Meisch, 2000). Although the water temperature apparently played a minor role, higher air temperatures typically cause stronger evaporation, and thus, higher $\delta^{18}O_{water}$ values of water and ostracod valves (Henderson and Holmes, 2009). Thus, we relate these $\delta^{18}O_{eq.cal}$

https://doi.org/10.5194/egusphere-2025-5999
Preprint. Discussion started: 7 January 2026

variations observed within the wetland-lake, wetland and wetland-alluvial plain intervals to the different $\delta^{18}O_{water}$ values of host waters (including lake and river waters) in the study area during the Early Pleistocene. Fan et al. (2014) reported that the modern $\delta^{18}O_{water}$ values of lake water in the Qarhan Salt Lake, Qaidam Basin, range between -8.5 and -4.9 ‰ (average -6.7 ‰) which are significantly higher than those of the river waters (including Golmud River and Nuomuhong River) flowing to Qarhan Lake, ranging from -11.8 to -8.8 ‰ (average -10.3 ‰). Fan et al. (2014) suggested that the higher $\delta^{18}O_{water}$ values of the lake water resulted from strong evaporation processes. Comparable isotopic variations have been also reported in the spring, river, and lake waters of the Lake Hulun Basin, Inner Mongolia (Han et al., 2019). According to their study, the average $\delta^{18}O_{water}$ values for spring, river, and lake waters recorded during 2017 were -11.9, -10.4, and -7.3 ‰, respectively. Drawing on these modern regional isotopic data as an analogous framework, the lowest and moderately higher average $\delta^{18}O_{eq.cal}$ values observed in the wetland and wetland-alluvial plain intervals probably correspond to waterbodies with minimal evaporative influence, potentially mirroring the stable isotopic signatures of spring and river waters, respectively. Conversely, the highest $\delta^{18}O_{eq.cal}$ values observed in wetland-lake intervals may reflect waterbody subjected to intense evaporation, analogous to lake waters. However, the effects of aridity and evaporation on the modern saline Qarhan Lake in the hyper-arid Qaidam Basin and in the higher latitude Lake Hulun Basin probably exceed those that affected the waterbodies of the Early Pleistocene Nihewan Basin.

To conclude, the Early Pleistocene Nihewan Basin was apparently a hydrologically closed basin, where prolonged water-residence time facilitated evaporative ^{18}O enrichment (Li and Ku, 1997; Paprocka, 2007). Consequently, the $\delta^{18}O_{eq.cal}$ variability reflects the amount of precipitation relative to the evaporation (i.e., the P/E ratio) or effective moisture and air humidity changes, and the more open (open wetland, alluvial plain) or closed (in-stream wetland, lake) nature of the waterbody at the section location (Gasse et al., 1996). Considering the variations in depositional facies reconstructed in the NH-T section in which the evaporation appears to be the dominant control, lower $\delta^{18}O_{eq.cal}$ values in the flowing stream/river waters probably resulted from drier conditions, whilst higher $\delta^{18}O_{eq.cal}$ values in more standing lake and wetland waters resulted from wetter conditions (Fig. 4).

In a closed basin, $\delta^{13}C_{ost}$ values track the regional hydrological balance and are mainly influenced by the $\delta^{13}C$ values of dissolved inorganic carbon (DIC) in the water column (Leng and

Marshall, 2004). Enhanced pCO_2 exchange between atmosphere and DIC under warm/humid conditions reduces pCO_2 dissolution, increasing $\delta^{13}C_{DIC}$ values (Leng and Marshall, 2004). Additionally, aquatic vegetation preferentially incorporates ^{12}C during photosynthesis, further enriching DIC in ^{13}C (Liu et al., 2015). However, interpreting $\delta^{13}C_{ost}$ values is complex due to the dominant influence of $\delta^{13}C_{DIC}$ and small-scale spatial heterogeneities in the ostracod's ambient water, driven by algal and aquatic plant growth and organic matter degradation (Decrouy et al., 2011). The $\delta^{13}C_{DIC}$ values may be also controlled by the inorganic input of carbon into the waterbody. Thus, $\delta^{13}C_{eq.cal}$ data can only be indirectly used for the inference of biological activities including photosynthetic productivity, and temperatures (Zanchetta et al., 2007). Higher $\delta^{13}C_{eq.cal}$ values in the NH-T section probably indicate increased biogenic productivity, driven by higher air temperatures, and/or enhanced evaporation effects in more standing lake or wetland waters, indicating wetter conditions (Fig. 4). Conversely, lower values suggest reduced biogenic productivity in the flowing stream/river waters, reflecting drier conditions (Fig. 4).

By combining these new $\delta^{18}O_{eq.cal}$ and $\delta^{13}C_{eq.cal}$ records with the reconstructed EAM climate changes between warm, humid interglacials, and cold, dry glacials based on the grain-size end-member (EM) dataset of the same NH-T section (Fig. 4, Fig. 5; Moghazi et al., 2024b), we provide a detailed picture of the hydrological changes during ca. 1.67-0.78 Ma.

5.1.1 Evolution between 1.67 to 1.30 Ma, the pre-MPT period

The depositional facies at the NH-T section represent six cycles of changing hydrodynamic conditions from 1) wetland-lake (ca. 1.67-1.52 Ma), 2) wetland (ca. 1.52-1.38 Ma), 3) wetland-alluvial plain (ca. 1.38-1.30 Ma), 4) wetland-lake (ca. 1.30-1.08 Ma), 5) wetland-alluvial plain (ca. 1.08-0.90 Ma), to 6) wetland-lake conditions (ca. 0.90-0.78 Ma) (Fig. 5; Moghazi et al., 2024a).

Wetland-lake interval (ca. 1.67-1.52 Ma)

In this interval, the $\delta^{18}O_{eq.cal}$ and $\delta^{13}C_{eq.cal}$ values are covariant with *r* value = 0.5. High $\delta^{18}O_{eq.cal}$ and moderately high $\delta^{13}C_{eq.cal}$ values dominate, punctuated by occasional excursions of moderately low to low values relative to the overall average and standard deviation ($\delta^{18}O_{eq.cal}$ -4.3 ± 2.15 ‰, and $\delta^{13}C_{eq.cal}$ -3.0 ± 2.9 ‰). In contrast to the highly variable $\delta^{18}O_{eq.cal}$ values, $\delta^{13}C_{eq.cal}$ values show gradually increasing trend (Fig. 5). The dominance of high or moderately high values indicates that wetter conditions with more standing waters, higher evaporation effects and increased biogenic productivity prevailed. The EM data support the interpretation of the stable

https://doi.org/10.5194/egusphere-2025-5999
Preprint. Discussion started: 7 January 2026

isotope data, indicating an intensified EASM, with apparently increased regional precipitation and elevated water level. Following the cycle-by-cycle correlation between the chronology of loess-paleosol record on CLP and the higher-resolution EM record of NH-T section and additional orbital tuning to astronomical solution (Fig. 5; Moghazi et al., 2024b; Laskar et al., 2004), this wetland-lake interval corresponds to the paleosols S_{23}-S_{21} and loess L_{23}-L_{22} deposits.

Wetland interval (ca. 1.52-1.38 Ma)

The covariance of $\delta^{18}O_{eq.cal}$ and $\delta^{13}C_{eq.cal}$ strengthens in this interval with *r* value = 0.8. The $\delta^{18}O_{eq.cal}$ values remain highly variable, while $\delta^{13}C_{eq.cal}$ values show an overall decrease trend towards the top of the interval (Fig. 5). The fluctuations between low and high $\delta^{18}O_{eq.cal}$ and $\delta^{13}C_{eq.cal}$ values indicate changes in the hydrological state, shifting back and forth between flowing and standing waters in contrast to the earlier wetland-lake interval when standing waters prevailed most of the time. $\delta^{18}O_{eq.cal}$ and $\delta^{13}C_{eq.cal}$ minima are lower than observed in the earlier wetland-lake interval, suggesting drier conditions and more open water with reduced evaporation effects and reduced biogenic productivity, especially near the top of the interval. This is consistent with EM data that show mixing EAM conditions with the slight dominance of EAWM conditions. This interval synchronously occurred with the L_{21}-L_{18} and S_{20}-S_{18} periods on CLP.

Wetland-alluvial plain interval (ca 1.38-1.30 Ma)

The $\delta^{18}O_{eq.cal}$ and $\delta^{13}C_{eq.cal}$ values in this interval maintain a strong covariance of *r* value = 0.8. The dominating high $\delta^{18}O_{eq.cal}$ and moderately high $\delta^{13}C_{eq.cal}$ values, along with the gradually increasing $\delta^{13}C_{eq.cal}$ trend, indicate a return to a more stagnant setting and higher water-residence time probably due to intensified wetter climatic conditions accompanied by increased biogenic productivity. EM data confirm the stronger influence of the EASM but indicate also locally increased input of terrestrial materials (Fig. 5). Based on the dominance of the high $\delta^{18}O_{eq.cal}$ values in this interval which probably result from strong effects of evaporative enrichment, sediments likely accumulated in an in-stream wetland with dense vegetation (Mischke et al., 2022) and slow water flow. The reconstructed in-stream wetland was apparently more strongly affected by evaporation than the open-basin wetland inferred for the sediments below in the NH-T section (Moghazi et al., 2024a). The timeframe of this interval corresponds to the S_{17}-S_{16} and L_{17} periods on CLP.

5.1.2 Evolution between ca. 1.30 to 0.78 Ma, the MPT period

https://doi.org/10.5194/egusphere-2025-5999
Preprint. Discussion started: 7 January 2026

Wetland-lake interval (ca. 1.30-1.08 Ma)

The $\delta^{18}O_{eq.cal}$ and $\delta^{13}C_{eq.cal}$ values here are not correlated (*r* value = 0.1). However, the dominance of moderately high $\delta^{18}O_{eq.cal}$ values in this interval indicates a high water-residence time, resulting in strong evaporative effects. More standing rather than flowing waters at the NH-T section location reflect dominantly wetter climate conditions. The concurrently moderately high to high $\delta^{13}C_{eq.cal}$ values suggest relatively increased biogenic productivity in comparison to the wetland-lake interval at the section's base. Although a strong $\delta^{18}O$-$\delta^{13}C$ covariance typically indicates a hydrologically-closed lake (Talbot, 1990), a low or absent covariance in such closed systems may either imply a stabilized lake level or a period of elevated pCO_2 (Li and Ku, 1997). We favor the interpretation of exceptionally higher pCO_2 concentrations in this interval as the absent covariance is accompanied by higher $\delta^{13}C_{eq.cal}$ values, especially at the top of the interval. The EM data support the interpretation of the stable isotope data because they indicate a transition from the dominance of EAWM conditions in the lower part to the dominance of EASM conditions in the middle and upper part of this interval (Moghazi et al., 2024b). The wetland-lake interval corresponds to the timeframe of L_{15}-L_{13} and S_{14}-S_{12} deposits on CLP.

Wetland-alluvial plain interval (ca. 1.08-0.90 Ma)

The $\delta^{18}O_{eq.cal}$ and $\delta^{13}C_{eq.cal}$ values of this interval are strongly positively correlated with *r* value = 0.8. The fluctuations between low and moderately high $\delta^{18}O_{eq.cal}$ and low and high $\delta^{13}C_{eq.cal}$ values suggest hydrological state changes between flowing and standing waters, probably reflecting high climate variability. The $\delta^{18}O_{eq.cal}$ and $\delta^{13}C_{eq.cal}$ minima and maxima are less extreme compared to the large stable isotope shifts observed in the wetland interval (ca. 1.52-1.38 Ma), suggesting shorter water residence times and weaker evaporative effects (Fig. 5). Also, relatively large oscillations of the EMs suggest fluctuating EAWM and EASM conditions. This interval aligns with the L_{12}-$L_{9\text{-}2}$ and S_{11}-S_9 periods on CLP (Fig. 5).

Wetland-lake interval (ca. 0.90-0.78 Ma)

The $\delta^{18}O_{eq.cal}$ and $\delta^{13}C_{eq.cal}$ values here are covariant again with *r* value = 0.7. Moderately high to high $\delta^{18}O_{eq.cal}$ and $\delta^{13}C_{eq.cal}$ values predominate this interval, reflecting the dominance of standing waters as a result of wetter climate with intensified monsoonal precipitation, enhanced evaporation effects, and elevated biogenic productivity. The EM data agree with this interpretation indicating prevailing EASM conditions for the middle and upper part of the interval. This uppermost wetland-lake interval correlates to the $L_{9\text{-}1}$ and S_8-S_7 periods on CLP (Fig. 5).

https://doi.org/10.5194/egusphere-2025-5999
Preprint. Discussion started: 7 January 2026

5.2 The NH-T stable isotope record and regional climate change

To assess whether the stable isotope variations recorded in the NH-T section reflect basin-specific hydrological dynamics or include regional climate signal, we here compare these variations with established marine and terrestrial palaeoclimatic records from the South China Sea (SCS) and CLP.

Qian et al. (2024) suggested that the change in the marine-land temperature gradients (ΔT) possibly affected the hydroclimate in East Asia. They observed shifts in the East Asia hydroclimate from overall dry to wet conditions together with increased ΔT. Interestingly, we also noticed that the $\delta^{18}O_{eq.cal}$ variations apparently track similar patterns of change in ΔT which might be indicative of the available moisture transported to the land. This ΔT typically fuels the EASM circulation. ΔT is calculated here from the difference between sea surface temperature (SST) at the Ocean Drilling Program (ODP) site 1146 in the SCS and land-surface temperature (LST) at the Lingtai section of CLP (Fig. 5; Clemens and Prell, 2003; Lu et al., 2022).

The concurrence of the $\delta^{18}O_{eq.cal}$ maximum at 12 m above the section's base with the EM-inferred strengthened EASM, the S_{22} interglacial on the CLP and a prominent increase in ΔT at ca. 1.55 Ma suggests that an EASM-driven precipitation increase led to a wetter climate in the monsoon region including Nihewan Basin. Moreover, Wang et al. (2004) reported a period of $\delta^{13}C$ maxima during 1.65-1.55 Ma at ODP site 1143 in the SCS, aligning with the dominance of higher $\delta^{18}O_{eq.cal}$ and gradually increasing $\delta^{13}C_{eq.cal}$ values in the wetland-lake interval (ca. 1.67-1.52 Ma) (Fig. 5). Similarly, Da et al. (2015) observed a brief increase in pCO_2 concentrations on CLP between ca. 1.6 and 1.5 Ma.

The highly variable $\delta^{18}O_{eq.cal}$ and gradually decreasing $\delta^{13}C_{eq.cal}$ values in the wetland interval from ca. 1.52-1.38 Ma align with the decrease in ΔT relative to the earlier wetland-lake interval (Fig. 5). Thus, a regional shift to colder and drier conditions is inferred. The three main $\delta^{18}O_{eq.cal}$ maxima of the interval correlate with the S_{20}-S_{18} periods, and the comparison with the variations in ΔT indicates S_{18} as the time of stronger EASM-driven precipitation in comparison to S_{20} and S_{19}.

A return to generally wetter conditions is reflected by high $\delta^{18}O_{eq.cal}$ and increasing $\delta^{13}C_{eq.cal}$ values in the in-stream wetland interval (ca 1.38-1.30 Ma), coinciding with a period of high ΔT. The $\delta^{18}O_{eq.cal}$ maxima aligned with S_{17} and S_{16} at 1.36 and 1.32 Ma match a strong and a moderate ΔT peak, respectively, supporting the inference of higher EASM-driven precipitation (Fig. 5).

https://doi.org/10.5194/egusphere-2025-5999
Preprint. Discussion started: 7 January 2026

The $\delta^{18}O_{eq.cal}$ minima and maxima in the following wetland-lake interval (ca. 1.30-1.08 Ma), corresponding to S_{14} and S_{13}, respectively, match with a similar pattern of variation in ΔT. This suggests the gradual intensification of EASM-driven precipitation, especially towards the top of the interval (Fig. 5).

The wetland-alluvial plain interval (ca. 1.08-0.90 Ma) aligns with a decreasing ΔT trend, reflecting reduced moisture transport to northern latitudes. The early stage of this interval was marked by an episode of increased $\delta^{18}O_{eq.cal}$ and $\delta^{13}C_{eq.cal}$ values. This episode coincides with a reported period of $\delta^{13}C$ maxima during 1.04-0.97 Ma at ODP site 1143 in the SCS (Fig. 5; Wang et al., 2004). Wang et al. (2004) noticed that the timing of the MPT with expansion of the ice sheets was following this period of inferred high CO_2 levels in the global ocean. We also noticed a following pronounced $\delta^{18}O_{eq.cal}$ minimum during the S_9 period correlates with a lower ΔT (Fig. 5). This feature probably resembles Weak Monsoon Intervals (WMIs) documented in speleothem records and attributed to ice-sheet dynamics in the Northern Hemisphere (Ziegler et al., 2010).

The increasing $\delta^{18}O_{eq.cal}$ and $\delta^{13}C_{eq.cal}$ values of the uppermost wetland-lake interval (ca. 0.9-0.78 Ma) correspond to a rising ΔT, pointing to enhanced EASM-driven precipitation (Fig. 5). Moreover, a $\delta^{18}O_{eq.cal}$ maximum during the S_8 period corresponds with high ΔT. This inference is supported by a reported increase in pCO_2 on CLP (Yamamoto et al., 2022).

5.3 Relationship between Early Pleistocene hydrological changes and hominin occupation

Archaeological excavations in the Nihewan Basin have uncovered hominin-produced stone tools dating back from ca.1.66-0.4 Ma (Dennell, 2013). Throughout this timeframe, the basin sustained mixed grassland and woodland habitats (Ao et al. 2013a). However, the archaeological record is not continuous, showing significant gaps between 1.5-1.4 Ma, 1.3-1.2 Ma, 1.0-0.9 Ma, and 0.8-0.4 Ma (Yang et al., 2019). Sun et al. (2018) suggested that these hiatuses were probably due to the inhospitable climatic conditions in northern latitudes, in contrast to the more continuous record found in southern China.

The characteristics of the waterbodies in the northeastern part of the basin apparently changed from hydrologically closed systems during wetter conditions and accompanied by increased productivity in the wetland-lake interval ca. 1.67-1.52 Ma, shifting to mixed hydrological conditions when the climate became steadily drier in the wetland interval ca. 1.52-1.38 Ma. Then, a return to a hydrologically-closed system with wetter conditions and enhanced productivity occurred in an in-stream wetland (ca. 1.38-1.30 Ma). At the oldest well-dated site, Majuangou (1.66-1.32 Ma), the pollen assemblage shows two different phases: one with forest/woodland dominance and the other with open grassland dominance (Potts and Faith, 2015). This trend towards increasing aridity is further supported by findings from the Xiantai site (1.36 Ma), where pollen are dominated by *Artemisia* and Chenopodiaceae, indicating a grassland environment and that the climate gradually became drier (Deng et al., 2006). In contrast, a brief warm and wet interval is evidenced at the Banshan site (1.324-1.318 Ma), characterized by a predominating *Pinus* forest during the period of human activity (Yang et al., 2022). This implies that the shifts in our stable isotope data are corroborated by pollen data from these early sites in the basin.

The inferred habitats range from the open grasslands at Feiliang (1.2 Ma; Pei et al., 2017) to the more humid forest-grassland mosaic at Donggutuo (1.10 Ma; Pei et al., 2009). This inference aligns with our findings which indicate progressively wetter conditions and increased productivity during the wetland-lake interval ca. 1.30-1.08 Ma. In contrast, the stable isotope results of Xu et al. (2023) suggest an opposite pattern, shifting from a wet and closed pure C_3 vegetation prior to 1.2 Ma, to drier and more open C_3/C_4 mixed vegetation during 1.2-1.1 Ma.

Our stable isotope data reveal a high climate variability, alternating between wetter and drier climate conditions during the wetland-alluvial plain interval ca. 1.08-0.90 Ma. Between 1.1 and 1.0 Ma, the density of stone artifacts increased, and lithic technology became more advanced (Fig. 5; Yang et al., 2021). We therefore associate the increased toolmaking skills and technological innovations of hominins with the wetter climatic phases in the transition from the end of the wetland-lake interval ca. 1.30 to 1.08 Ma and the early stage of the wetland-alluvial plain interval ca. 1.08-0.9 Ma (Fig. 5). The archaeological gap between 1.0 and 0.90 Ma coincides with a pronounced drying trend inferred from our stable isotope data (Fig. 5; Yang et al., 2021). Following this gap, the stable isotope evidence indicates that wetter conditions with higher biogenic productivity prevailed during ca. 0.9-0.78 Ma. Corresponding to this wetter period, artefacts are reported from the Nihewan Basin again (Yang et al., 2021).

Our findings are broadly consistent with Dennell's (2013) suggestion that hominins likely occupied the basin during the warmer, favorable periods and avoided it under significantly colder ones (Fig. 4, Fig. 5).

https://doi.org/10.5194/egusphere-2025-5999
Preprint. Discussion started: 7 January 2026

6. CONCLUSIONS

- This study presents the first long-term stable isotope record of the Early Pleistocene Nihewan Basin.
- The strong covariance of $\delta^{18}O_{eq.cal}$ and $\delta^{13}C_{eq.cal}$ values implies that the Early Pleistocene Nihewan Basin was mostly hydrologically closed.
- The $\delta^{18}O_{eq.cal}$ and $\delta^{13}C_{eq.cal}$ data show that water bodies in the basin were strongly affected by evaporation.
- Thus, the $\delta^{18}O_{eq.cal}$ variability reflects the local hydrological state at the section location between closed (more standing waters, in-stream wetland, lake) and open (more flowing waters, open wetland, alluvial plain) settings instead of regional P/E ratios alone.
- The concurrence of high $\delta^{18}O_{eq.cal}$ and $\delta^{13}C_{eq.cal}$ values and the increase in ΔT is indicative of an increase in the proportion of EASM-driven precipitation which led to wetter climate and increased biogenic productivity, whereas low values reflect decreased EASM-driven precipitation and drier climate and reduced biogenic productivity.
- In comparison with the synthetic Early Pleistocene artefact record from the basin, inferred hominin occupation mostly coincided with periods of higher $\delta^{18}O_{eq.cal}$ and $\delta^{13}C_{eq.cal}$ values. Thus, hominins were more present during wetter climate periods when more standing waters bodies had formed in the Nihewan Basin.

Code/Data availability

The raw data will be made available upon request.

Author contribution

AH: Methodology, Formal Analysis, Visualization, Writing–original draft, Writing–review and editing. HZ: Conceptualization, Writing–review and editing. CZ: Writing–review and editing. BS: Methodology, Formal Analysis, Writing–review and editing. SM: Conceptualization, Supervision, Writing–review and editing, Funding acquisition.

Competing interests

The authors declare that they have no known competing financial interests or personal relationships that could have appeared to influence the work reported in this paper.

Acknowledgments

Funding for this research was provided by the University of Iceland Research Fund and the Icelandic Centre for Research (RANNÍS, grant number 185360-052).

References

Ao, H., Dekkers, M., An, Z., Xiao, G., Li, Y., Zhao, H., Qiang, X., Chang, H., Chang, Q. and Wu, D. (2013). Magnetostratigraphic evidence of a mid-Pliocene onset of the Nihewan Formation-implications for early fauna and hominid occupation in the Nihewan Basin, North China. Quat. Sci. Rev. 59, 30-42. https://doi.org/10.1016/j.quascirev.2012.10.025

Barbour, G. (1924). Preliminary observations in the Kalgan area. Bull. Geol. Soc. China 3, 153-68. https://doi.org/10.1111/j.1755-6724.1924.mp3002009.x

Barbour, G., Licent, E. and Teilhard de Chardin, P. (1927). Geological study of the deposits of the Sangkanho Basin. Bull. Geol. Soc. China 5, 263-278.

Bi, Y., Pang, E., Sun, Y., Liu, Y., Bian, Q., Liu, S., Shen, Z., Xiong, J., Zhang, H., Hao, Q. and Deng, C. (2022). Magnetostratigraphy of the fluvio-lacustrine sequence of core DY-1 in the Datong Basin and its implications for the evolution of the Shanxi Rift System in northern China. Palaeogeogr. Palaeoclimatol. Palaeoecol. 599, 111063. https://doi.org/10.1016/j.palaeo.2022.111063

Blazina, T., Sun, Y., Voegelin, A., Lenz, M., Berg, M. and Winkel, L. (2014). Terrestrial selenium distribution in China is potentially linked to monsoonal climate. Nat. Commun. 5, 4717. https://doi.org/10.1038/ncomms5717

Börner, N., De Baere, B., Akita, L.G., Francois, R., Jochum, K.P., Frenzel, P., Zhu, L. and Schwalb, A. (2017). Stable isotopes and trace elements in modern ostracod shells: implications for reconstructing past environments on the Tibetan Plateau, China. J. Paleolimnol. 58, 191-211. https://doi.org/10.1007/s10933-017-9971-1

Clemens, S. and Prell, W. (2003). Data report: oxygen and carbon isotopes from site 1146, northern South China Sea. In: Prell, W.L., Wang, P., Blum, P., Rea, D. and Clemens, S. (Eds.), Proc. Ocean Drill. Program Sci. Results 184, 1-8.

https://doi.org/10.5194/egusphere-2025-5999
Preprint. Discussion started: 7 January 2026

Da, J., Zhang, Y.G., Wang, H., Balsam, W. and Ji, J. (2015). An Early Pleistocene atmospheric CO_2 record based on pedogenic carbonate from the Chinese loess deposits. Earth Planet. Sci. Lett. 426, 69-75. https://doi.org/10.1016/j.epsl.2015.05.053

Decrouy, L., Vennemann, T. and Ariztegui, D. (2011). Controls on ostracod valve geochemistry, Part 1: Variations of environmental parameters in ostracod (micro-) habitats. Geochim. Cosmochim. Acta 75, 7364-7379. https://doi.org/10.1016/j.gca.2011.09.009

Deng, C., Shaw, J., Liu, Q., Pan, Y., Zhu, R. (2006a). Mineral magnetic variation of the Jingbian loess/paleosol sequence in the northern Loess Plateau of China: implications for Quaternary development of Asian aridification and cooling. Earth Planet Sci. Lett. 241, 248–259. https://doi.org/10.1016/j.epsl.2005.10.020

Deng, C., Wei, Q., Zhu, R., Wang, H., Zhang, R., Ao, H., Chang, L. and Pan, Y. (2006b). Magnetostratigraphic age of the Xiantai Paleolithic site in the Nihewan Basin and implications for early human colonization of northeast Asia. Earth Planet. Sci. Lett. 244, 336-348. https://doi.org/10.1016/j.epsl.2006.02.001

Deng, C., Xie, F., Liu, C., Ao, H., Pan, Y., Zhu, R. (2007). Magnetochronology of the Feiliang Paleolithic site in the Nihewan Basin and implications for early human adaptability to high northern latitudes in East Asia. Geophys. Res. Lett. 34, 1-6. https://doi.org/10.1016/j.quaint.2012.02.012

Deng, C., Zhu, R., Zhang, R., Ao, H. and Pan, Y. (2008). Timing of the Nihewan formation and faunas. Quat. Res. 69, 77-90. https://doi.org/10.1016/j.yqres.2007.10.006

Dennell, R. (2013). The Nihewan Basin of North China in the early Pleistocene: continuous and flourishing, or discontinuous, infrequent and ephemeral occupation? Quat. Int. 295, 223-236. https://doi.org/10.1016/j.quaint.2012.02.012

Fan, Q., Ma, H., Wei, H., Shan, F., An, F., Xu, L. and Madsen, D. (2014). Late Pleistocene paleoclimatic history documented by an oxygen isotope record from carbonate sediments in Qarhan Salt Lake, NE Qinghai-Tibetan Plateau. J. Asian Earth Sci. 85, 202-209. https://doi.org/10.1016/j.jseaes.2014.02.003

https://doi.org/10.5194/egusphere-2025-5999
Preprint. Discussion started: 7 January 2026

Gasse, F., Fontes, J., Van Campo, E., Wei, K. (1996). Holocene environmental changes in Bangong Co basin (Western Tibet). Part 4: discussion and conclusions. Palaeogeogr. Palaeoclimatol. Palaeoecol. 120, 79-92. https://doi.org/10.1016/0031-0182(95)00035-6

Han, Z., Li, X., Wang, Y., Wang, X., Yi, S. and Lu, H. (2016). Tectonically-controlled infilling of the eastern Nihewan Basin, North China, since the middle Pleistocene. Sci. China Earth Sci. 59, 1378-1389. https://doi.org/10.1007/s11430-016-5264-1

Han, Z., Shi, X., Jia, K., Sun, B., Zhao, S. and Fu, C. (2019). Determining the discharge and recharge relationships between lake and groundwater in Lake Hulun using hydrogen and oxygen isotopes and chloride ions. Water 11, 264. https://doi.org/10.3390/w11020264

Henderson, A. and Holmes, J. (2009). Palaeolimnological evidence for environmental change over the past millennium from Lake Qinghai sediments: a review and future research prospective. Quat. Int. 194, 134-147. https://doi.org/10.1016/j.quaint.2008.09.008

Holmes, J. and Chivas, A. (2002). The Ostracoda: applications in Quaternary research. Geophys. Monogr. Ser. 131. https://doi.org/10.1029/131GM10

Kim, S. and O'Neil, J. (1997). Equilibrium and nonequilibrium oxygen isotope effects in synthetic carbonates. Geochim. Cosmochim. Acta 61, 3461-3475. https://doi.org/10.1016/S0016-7037(97)00169-5

Laskar, L., Robutel, P., Joutel, F., Gastineau, M., Correia, A. and Levard, B. (2004). A long-term numerical solution for insolation quantities of the Earth. Astron. Astrophys. 428, 261-285. https://doi.org/10.1051/0004-6361:20041335

Leng, M. and Marshall, J. (2004). Palaeoclimate interpretation of stable isotope data from lake sediment archives. Quat. Sci. Rev. 23, 811-831. https://doi.org/10.1016/j.quascirev.2003.06.012

Li, H. and Ku, T. (1997). $\delta^{13}C$-$\delta^{18}C$ covariance as a paleohydrological indicator for closed-basin lakes. Palaeogeogr. Palaeoclimatol. Palaeoecol. 133, 69-80. https://doi.org/10.1016/S0031-0182(96)00153-8

Li, R., Qiao, J., Qiu, W., Zhai, Q. and Li, Y. (2000). Soluble salt deposit in the Nihewan beds and its environmental significance. Sci. China Ser. D Earth Sci. 43, 464-479. https://doi.org/10.1007/BF02875308

https://doi.org/10.5194/egusphere-2025-5999
Preprint. Discussion started: 7 January 2026

Li, R., Yu, S., Sun, P., He, S., Yuan, Y., Xiong, Z. (2015). Characteristics of $\delta^{13}C$ in typical aquatic plants and carbon sequestration by plant photosynthesis in the Banzhai catchment, Maolan of Guizhou Province. Carsol. Sin. 34, 9-16. (Chinese with English abstract).

Liu, P., Deng, C., Li, S., Zhu, R. (2010). Magnetostratigraphic dating of the Huojiadi paleolithic site in the Nihewan Basin, north China. Palaeogeogr. Palaeoclimatol. Palaeoecol. 298, 399408. https://doi.org/10.1016/j.palaeo.2010.10.027

Lu, H., Liu, W., Yang, H., Leng, Q., Liu, Z., Cao, Y., Hu, J., Sheng, W., Wang, H., Wang, Z. and Zhang, Z. (2022). Decoupled land and ocean temperature trends in the early-middle Pleistocene. Geophys. Res. Lett. 49, e2022GL099520. https://doi.org/10.1029/2022GL099520

Meisch, C. (2000). Freshwater Ostracoda of Western and Central Europe, Süßwasserfauna von Mitteleuropa 8/3. Heidelberg: Spektrum Akad. Verlag 522.

Min, L., and Chi, Z. Q. (2003). Quaternary geology of the Western Yangyuan Basin. Beijing: Geol. Publ. House.

Mischke, S., Kramer, M., Zhang, C., Shang, H., Herzschuh, U. and Erzinger, J. (2008). Reduced early Holocene moisture availability in the Bayan Har Mountains, northeastern Tibetan Plateau, inferred from a multi-proxy lake record. Palaeogeogr. Palaeoclimatol. Palaeoecol. 267, 59-76. https://doi.org/10.1016/j.palaeo.2008.06.002

Mischke, S., Lai, Z., Faershtein, G., Porat, N., Röhl, M., Braun, P., Kalbe, J. and Ginat, H. (2021). A Late Pleistocene wetland setting in the arid Jurf ed Darawish region in central Jordan. Front. Earth Sci. 9, 722435. https://doi.org/10.3389/feart.2021.722435

Moghazi, H., Zhao, H., Zhang, C., Eythorsdottir, E. and Mischke, S. (2024a). Early Pleistocene depositional and environmental conditions at Dachangliang, Nihewan Basin, NE China. Front. Earth Sci. 12. https://doi.org/10.3389/feart.2024.1335360

Moghazi, H., Zhao, H., Zhang, C., Omar, H., Eltijani, A. and Mischke, S. (2024b). The East Asian monsoon variability in the Nihewan Basin, northern China, during the Early Pleistocene: a grain size end-member modelling analysis. Quat. Sci. Rev. 346, 109022. https://doi.org/10.1016/j.quascirev.2024.109022

Mu, H., Xu, Q., Zhang, S., Hun, L., Li, M., Li, Y., Hu, Y. and Xie, F. (2015). Pollen-based quantitative reconstruction of the paleoclimate during the formation process of Houjiayao Relic Site in Nihewan Basin of China. Quat. Int. 374, 76-84. https://doi.org/10.1016/j.quaint.2015.02.019

Paprocka, A. (2007). Stable carbon and oxygen isotopes in recent sediments of Lake Wigry, NE Poland: implications for lake morphometry and environmental changes. Terr. Ecol. 1, 267-281. https://doi.org/10.1016/S1936-7961(07)01017-2

Pei, S., Li, X., Liu, D., Ma, N. and Peng, F. (2009). Preliminary study on the living environment of hominids at the Donggutuo site, Nihewan Basin. Chin. Sci. Bull. 54, 3896-3904. https://doi.org/10.1007/s11434-009-0646-9

Pei, S., Xie, F., Deng, C., Jia, Z., Wang, X., Guan, Y., Li, X., Ma, D. and de la Torre, I. (2017). Early Pleistocene archaeological occurrences at the Feiliang site, and the archaeology of human origins in the Nihewan Basin, North China. *PLoS One* 12, 0187251. https://doi.org/10.1371/journal.pone.0187251

Pei, S., Deng, C., de la Torre, I., Jia, Z., Ma, D., Li, X. and Wang, X. (2019). Magnetostratigraphic and archaeological records at the Early Pleistocene site complex of Madigou (Nihewan Basin): implications for human adaptations in North China. Palaeogeogr. Palaeoclimatol. Palaeoecol. 530, 176-189. https://doi.org/10.1016/j.palaeo.2019.05.014

Potts, R. and Faith, J. (2015). Alternating high and low climate variability: the context of natural selection and speciation in Plio-Pleistocene hominin evolution. J. Hum. Evol. 87, 5-20. https://doi.org/10.1016/j.jhevol.2015.06.014

Potts, R., Dommain, R., Moerman, J.W., Behrensmeyer, A.K., Deino, A.L., Riedl, S., Beverly, E.J., Brown, E.T., Deocampo, D., Kinyanjui, R. and Lupien, R. (2020). Increased ecological resource variability during a critical transition in hominin evolution. Sci. Adv. 43, 75-84. https://www.science.org/doi/10.1126/sciadv.abc8975

Qian, S., Xu, Q., Griffiths, M., Yang, H. and Xie, S. (2024). Decoupled terrestrial temperature and hydroclimate during the Plio-Pleistocene in the East Asian monsoonal region. Quat. Sci. Rev. 344, 108955. https://doi.org/10.1016/j.quascirev.2024.108955

https://doi.org/10.5194/egusphere-2025-5999
Preprint. Discussion started: 7 January 2026

Qiu, Z. (2000). Nihewan fauna and Q/N boundary in China (in Chinese with English abstract). Quat. Sci. 20, 142-154.

Schwalb, A. (2003). Lacustrine ostracodes as stable isotope recorders of late-glacial and Holocene environmental dynamics and climate. J. Paleolimnol. 29, 267-351. https://doi.org/10.1023/A:1024038429005

Schwalb, A., Dean, W., Güde, H., Hanisch, S., Sobek, S. and Wessels, M. (2013). Benthic ostracode $\delta^{13}C$ as sensor for early Holocene establishment of modern circulation patterns in Central Europe. Quat. Sci. Rev. 66, 112-122. https://doi.org/10.1016/j.quascirev.2012.10.032

Sun, J. (2005). Long-term fluvial archives in the Fen Wei Graben, central China, and their bearing on the tectonic history of the India-Asia collision system during the Quaternary. Quat. Sci. Rev. 24, 1279-1286. https://doi.org/10.1016/j.quascirev.2004.08.018

Sun, X., Lu, H., Wang, S., Xu, X., Zeng, Q., Lu, X., Lu, C., Zhang, W., Zhang, X. and Dennell, R. (2018). Hominin distribution in glacial-interglacial environmental changes in the Qinling Mountains range, central China. Quat. Sci. Rev. 198, 37-55. https://doi.org/10.1016/j.quascirev.2018.08.012

Talbot, M. (1990). A review of the palaeohydrological interpretation of carbon and oxygen isotopic ratios in primary lacustrine carbonates. Chem. Geol. Isot. Geosci. Sect. 80, 261-279. https://doi.org/10.1016/0168-9622(90)90009-2

Teilhard de Chardin, P. and Piveteau, J. (1930). Les mammifères fossiles de Nihowan (Chine). Ann. Paléontol. 19, 1-134

Tian, J., Wang, P., Cheng, X. and Li, Q. (2002). Astronomically tuned Plio–Pleistocene benthic $\delta^{18}O$ record from South China Sea and Atlantic-Pacific comparison. Earth Planet. Sci. Lett. 203, 1015-1029. https://doi.org/10.1016/S0012-821X(02)00923-8

Tian, J., Wang, P. and Cheng, X. (2004). Development of the East Asian monsoon and Northern Hemisphere glaciation: oxygen isotope records from the South China Sea. Quat. Sci. Rev. 23, 2007-2016. https://doi.org/10.1016/j.quascirev.2004.02.013

Tu, H., Luo, L., Deng, C., Ou, Z., Lai, Z., Shen, G., Bae, C. and Granger D. (2022). Isochron ^{26}Al/^{10}Be burial dating of the Xiashagou Fauna in the Nihewan Basin, northern China: implications for biogeography and early hominin dispersals. Quat. Sci. Rev. 283, 107447. https://doi.org/10.1016/j.quascirev.2022.107447

von Grafenstein, U., Erlenkeuser, H., Mu¨ller, H., Jouzel, J. and Johnsen, S. (1999). A mid-European decadal isotope-climate record from 15,500 to 5000 years BP. Science 284, 1654-1657. https://www.science.org/doi/10.1126/science.284.5420.1654

von Grafenstein, U., Eicher, U., Erlenkeuser, H., Ruch, P., Schwander, J. and Ammann, B. (2000). Isotope signature of the Younger Dryas and two minor oscillations at Gerzensee (Switzerland): palaeoclimatic and palaeolimnologic interpretation based on bulk and biogenic carbonates. Palaeogeogr. Palaeoclimatol. Palaeoecol. 159, 215-229. https://doi.org/10.1016/S0031-0182(00)00086-9

Wang, P., Tian, J., Cheng, X., Liu, C. and Xu, J. (2004). Major Pleistocene stages in a carbon perspective: the South China Sea record and its global comparison. Paleoceanography 19. https://doi.org/10.1029/2003PA000991

Wang, H., Deng, C., Zhu, R., Wei, Q., Hou, Y., Bo¨eda, E. (2005). Magnetostratigraphic dating of the Donggutuo and Maliang paleolithic sites in the Nihewan Basin, north China. Quat. Res. 64, 1-11. https://doi.org/10.1016/j.yqres.2005.04.001

Wang, P., Tian, J. and Lourens, L. (2010). Obscuring of long eccentricity cyclicity in Pleistocene oceanic carbon isotope records. Earth Planet. Sci. Lett. 290, 319-330. https://doi.org/10.1016/j.epsl.2009.12.028

Xie, F. and Cheng S. (1990). Palaeoliths excavation in Cenjiawan Village, Yangyuan County, Hebei Province. Acta Anthropol. Sin. 9, 265.

Xu, Z., Pei, S., Hu, Y., de la Torre, I. and Ma, D. (2021). Stable isotope analysis of mammalian enamel from the Early Pleistocene site of Madigou, Nihewan Basin: implications for reconstructing hominin paleoenvironmental adaptations in North China. Front. Earth Sci. 9, 789781. https://doi.org/10.3389/feart.2021.789781

Xu, Z., Pei, S., Hu, Y., de la Torre, I., Ma, D., Ye, Z. and Deng, C. (2023). Ecological shifts and hominin adaptations during the Mid-Pleistocene Climate Transition in Northeast Asia as evidenced by isotopic analysis ($\delta^{13}C$, $\delta^{18}O$) of mammalian enamel from early Paleolithic sites in the Nihewan Basin, China. Quat. Sci. Rev. 308, 108072. https://doi.org/10.1016/j.quascirev.2023.108072

Yamamoto, M., Clemens, S., Seki, O., Tsuchiya, Y., Huang, Y., O'ishi, R. and Abe-Ouchi, A. (2022). Increased interglacial atmospheric CO_2 levels followed the mid-Pleistocene Transition. Nat. Geosci. 15, 307-313. https://doi.org/10.1038/s41561-022-00918-1

Yang, S., Deng, C., Zhu, R. and Petraglia, M. (2019). The Paleolithic in the Nihewan Basin, China: evolutionary history of an early to late Pleistocene record in Eastern Asia. Evol. Anthropol. 29, 125-142. https://doi.org/10.1002/evan.21813

Yang, J., Zhang, Z., Li, Y., Wang, F., Fan, B., She, Z., Xie, H., Wang, S. and Da, S. (2022). Environment of the early Pleistocene Banshan Paleolithic site in the Nihewan Basin, north China. Front. Earth Sci. 10, 830798. https://doi.org/10.3389/feart.2022.830798

Yang, S., Wang, F.G., Xie, F., Yue, J., Deng, C., Zhu, R. and Petraglia, M. (2021). Technological innovations at the onset of the Mid-Pleistocene Climate Transition in high-latitude East Asia. Natl. Sci. Rev. 8. https://doi.org/10.1093/nsr/nwaa053

Young, C. (1950). "The Plio-Pleistocene boundary in China," Rep. 18th Int. Geol. Congr. (London: Wiley), 115-125.

Zanchetta, G., Drysdale, R., Hellstrom, J., Fallick, A., Isola, I., Gagan, M. and Pareschi, M. (2007). Enhanced rainfall in the Western Mediterranean during deposition of sapropel S1: stalagmite evidence from Corchia cave (Central Italy). Quat. Sci. Rev. 26, 279-286. https://doi.org/10.1016/j.quascirev.2006.12.003

Zhang, Z., Li, Y., Li, C., Xu, Q., Zhang, R., Ge, Y., Li, B., Deng, C., Li, Z. and Zhang, L. (2020). Pollen evidence for the environmental context of the early Pleistocene Xiashagou fauna of the Nihewan Basin, north China. Quat. Sci. Rev. 236, 106298. https://doi.org/10.1016/j.quascirev.2020.106298

Zhai, D., Xiao, J., Zhou, L., Wen, R., Chang, Z., Wang, X., Jin, X., Pang, Q. and Itoh, S. (2011). Holocene East Asian monsoon variation inferred from species assemblage and shell chemistry of the ostracodes from Hulun Lake, Inner Mongolia. Quat. Res. 75, 512-522. https://doi.org/10.1016/j.yqres.2011.02.008

Zhou, T., Li, H., Liu, Q., Li, R. and Sun X. (1991). Cenozoic Paleography Research of Nihewan Basin.

Zhu, R., Potts, R., Xie, F., Hoffman, K., Deng, C., Shi, C. D., Pan, Y., Wang, H., Shi, R., Wang, Y., Shi, G. and Wu, N. (2004). New evidence on the earliest human presence at high northern latitudes in Northeast Asia. Nature 431, 559-562. https://doi.org/10.1038/nature02829

Zhu, Z., Dennell, R., Huang, W., Wu, Y., Rao, Z., Qiu, S., Xie, J., Liu, W., Fu, S., Han, J. and Zhou, H. (2015). New dating of the *Homo erectus* cranium from Lantian (Gongwangling), China. J. Hum. Evol. 78, 144-157. https://doi.org/10.1016/j.jhevol.2014.10.001

Ziegler, M., Lourens, L., Tuenter, E., Hilgen, F., Reichart, G.J. and Weber, N. (2010). Precession phasing offset between Indian summer monsoon and Arabian Sea productivity linked to changes in Atlantic overturning circulation. Paleoceanography 25. https://doi.org/10.1029/2009PA001884

https://doi.org/10.5194/egusphere-2025-5999
Preprint. Discussion started: 7 January 2026

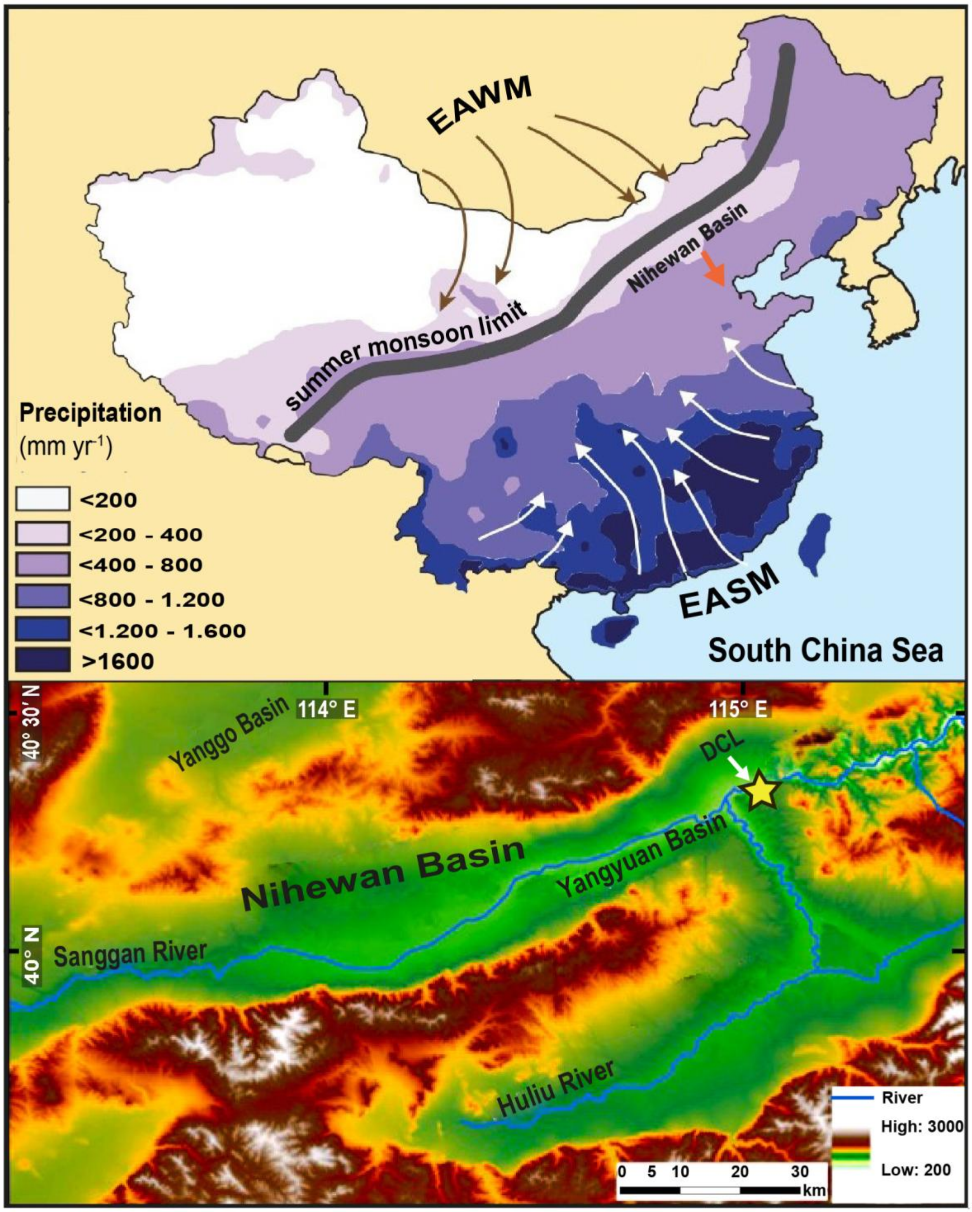

Figure 1 *Upper panel: mean precipitation distribution in China during 1980-2010 (modified after Blazina et al., 2014). Grey thick line = East Asian summer monsoon (EASM) limit. Wite arrows = EASM flow; Dark arrows = East Asian Winter Monsoon (EAWM); orange arrow = Position of Nihewan Basin. Lower panel: Nihewan Basin topography. Yellow star = Dachangliang (DCL) study site*

https://doi.org/10.5194/egusphere-2025-5999
Preprint. Discussion started: 7 January 2026

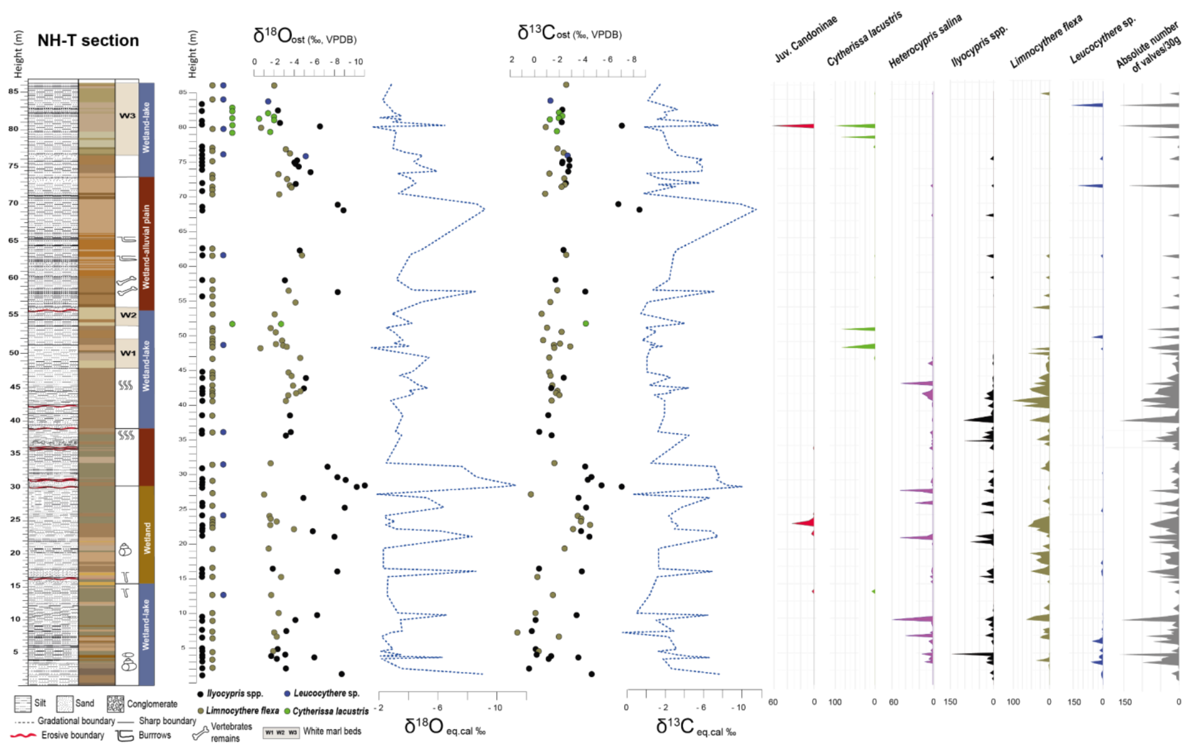

__Figure 2__ Stratigraphy of the sediment section NH-T, showing lithology, colour, positions of white marker layers (W1-W3), depositional settings (after Moghazi et al., 2024a), stratigraphic positions of ostracod valves used for stable isotope analysis ($\delta^{18}O_{ost}$ and $\delta^{13}C_{ost}$), the vital offset corrected $\delta^{18}O_{eq.cal}$ and $\delta^{13}C_{eq.cal}$ data, and the absolute abundance of ostracod valves per 30 g of sediment

https://doi.org/10.5194/egusphere-2025-5999
Preprint. Discussion started: 7 January 2026

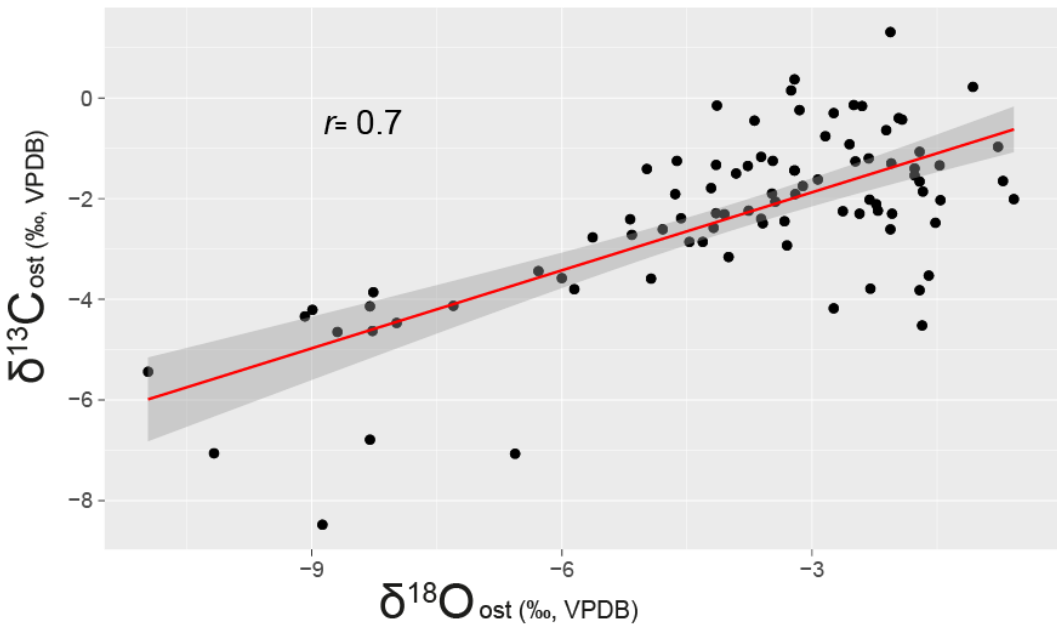

Figure 3 *Cross plot of the $\delta^{18}O_{ost}$ and $\delta^{13}C_{ost}$ data and correlation coefficient (r)*

https://doi.org/10.5194/egusphere-2025-5999
Preprint. Discussion started: 7 January 2026

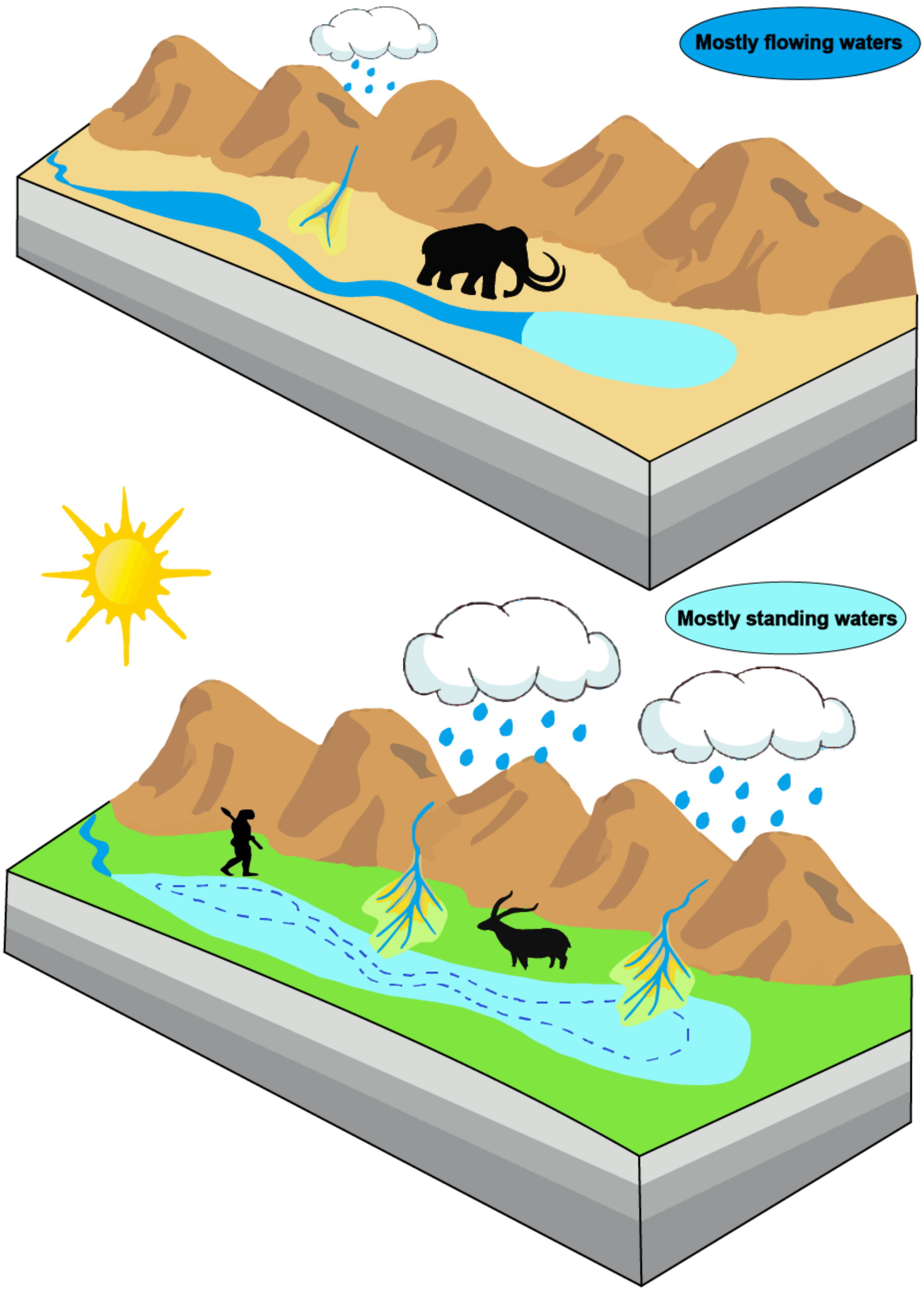

734 ***Figure 4*** *Schematic model showing the hydrological state shifts between standing and flowing waters in the Early Pleistocene Nihewan Basin*

https://doi.org/10.5194/egusphere-2025-5999
Preprint. Discussion started: 7 January 2026

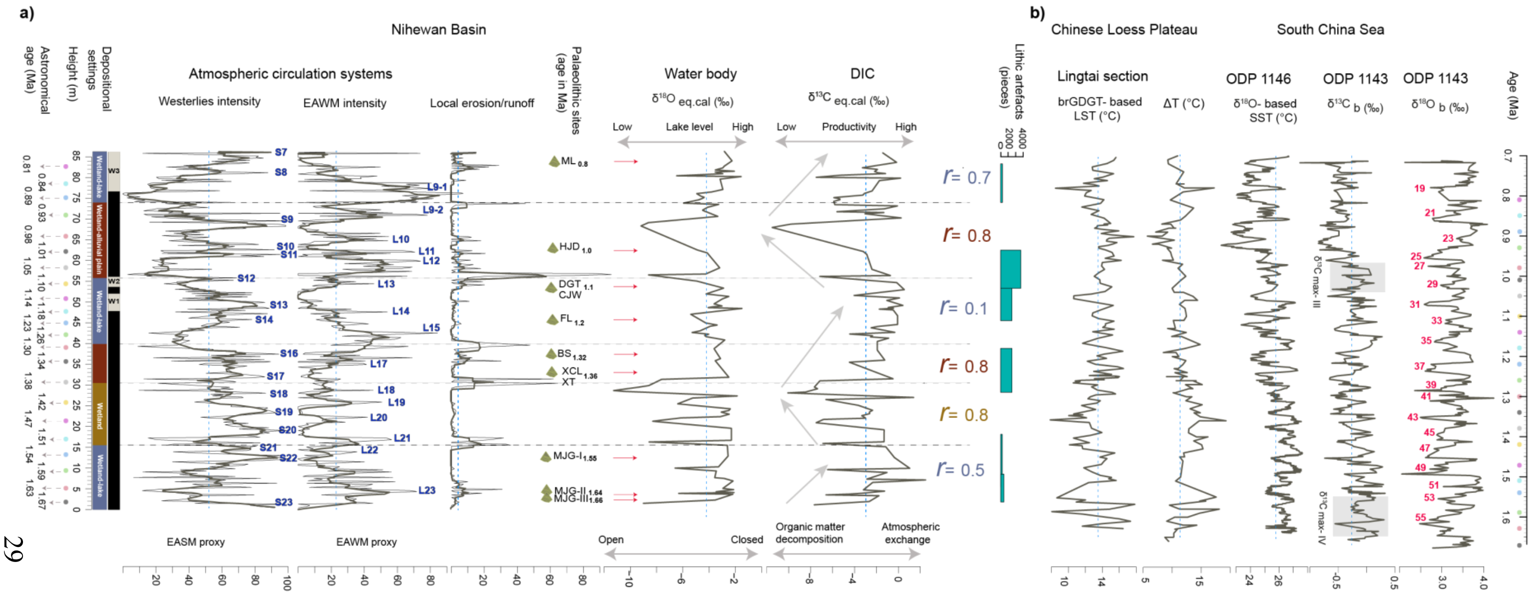

Figure 5 a) Variation in the relative abundance of end members (EMs) 1, 3 and 4 as proxies for EASM, EAWM and local runoff with the revised astronomical age of NH-T section (Moghazi et al. 2024b). The correlated S (palaeosol) and L (loess) periods of CLP are marked in blue (Moghazi et al. 2024b). Dashed horizontal lines mark the boundaries of six cycles of changing hydrodynamic conditions (Moghazi et al. 2024a). The Palaeolithic sites in the Nihewan Basin are MJG-III = Majuangou III (Zhu et al., 2004), MJG-II = Majuangou II (Zhu et al., 2004), MJG-I = Majuangou I (Zhu et al., 2004), XT = Xiantai (Deng et al., 2006a, 2006b), XCL = Xiaochangliang (Zhu et al., 2001), BS = Banshan (Zhu et al., 2004), FL = Feiliang (Deng et al., 2007), DGT = Donggutuo (Wang et al., 2005), CJW = Cenjiawan (Xie and Cheng, 1990), HJD = Huojiadi (Liu et al., 2010), ML = Maliang (Wang et al., 2005). Red arrows mark the concurrence between the Palaeolithic sites and higher $\delta^{18}O_{eq.cal}$ and $\delta^{13}C_{eq.cal}$ values. b) GDGT-derived LST on the CLP (Lu et al., 2022), the difference in sea and terrestrial temperatures (ΔT), $\delta^{18}O$-derived SST record of ODP site 1146 on the SCS (Clemens and Prell, 2003), benthic $\delta^{13}C_b$ and $\delta^{18}O_b$ records of ODP site 1143 on the SCS (Tian et al., 2002, 2004; Wang et al., 2004, 2010). Grey boxes mark the intervals of two $\delta^{13}C$ maxima identified in the $\delta^{18}O_b$ record of ODP site 1143: $\delta^{13}C_{max\text{-}III}$ (1.04-0.97 Ma) and $\delta^{13}C_{max\text{-}VI}$ (1.65-1.55 Ma) (Wang et al., 2004)